

# The Electrostatic Contribution to the Forward-Scattering Potential at a Space Charge Layer in High-Energy Electron Diffraction.

## I. Theory Neglecting the Effects of Fringing Fields

R. E. DUNIN-BORKOWSKI,\* W. O. SAXTON AND W. M. STOBBS

Department of Materials Science and Metallurgy, Pembroke Street, Cambridge CB2 3QZ, England.  
E-mail: red10@cam.ac.uk

(Received 27 September 1995; accepted 9 April 1996)

### Abstract

Expressions for the electrostatic potential at an interfacial space charge layer are determined using classical electrostatics, with particular reference to the use of phase-contrast techniques in transmission electron microscopy for characterizing such layers. Both the sensitivity of the potential to the detailed form of the charge distribution and the effect of the internal electric field on the strain within the material are discussed.

### 1. Introduction

A space charge layer at a grain boundary in an ionic solid (Yan, Cannon & Bowen, 1983; Ikeda & Chiang, 1993) or at an undepleted delta-doped layer in a semiconductor (Schubert, 1993) is generally characterized by the presence of a sheet of charged impurities or defects at the boundary and a broader distribution of oppositely charged free carriers. According to Poisson's equation, such charge-density variations give rise to changes in electrostatic potential within a material that remains electrically neutral overall. This suggests that it should be possible to quantify charge distributions at space charge layers in the transmission electron microscope (TEM) by using analytical techniques that are sensitive to local differences in potential. In particular, phase-contrast techniques such as Fresnel contrast analysis, *e.g.* Ross & Stobbs (1991), and electron holography, *e.g.* Tonomura (1992), can be applied provided that all other contributions to the specimen potential at the boundary, such as changes in electron scattering factor and density, are either negligible or well characterized.† The typical cross-sectional geometry required for TEM examination of a space charge layer is shown schematically in Fig. 1. Lin, Ravikumar, Rodrigues, Wilcox & Draivid (1995) have reported electron holographic obser-

vations of changes in potential with such origins at grain boundaries in Mn-doped SrTiO<sub>3</sub>, while Ikeda, Chiang, Garratt-Reed & Vander Sande (1993) have used the more indirect approach of measuring the total amount of Al, Ga and Nb segregating at grain boundaries in TiO<sub>2</sub> and inferring the corresponding boundary potentials. Dunin-Borkowski, Stobbs, Perovic & Wasilewski (1994) have shown that the magnitude of Fresnel contrast visible at delta-doped layers in specimens of Si and GaAs could not be accounted for by changes in composition, density or ionicity at the layers, but was consistent with the presence of space charge distributions. However, no work has yet been published on either the quantitative interpretation of the potential measured at a space charge layer or the sensitivity of the measured potential to the form of the original charge distributions.

The aim of this paper is to illustrate how classical solutions of Poisson's equation can be used to relate a TEM-measured potential at a space charge layer to the charge distributions that are present. The contribution to the strain within the material, which results from the presence of the electric field associated with these charge distributions and can affect both diffraction and phase contrast in a TEM image, is also determined.

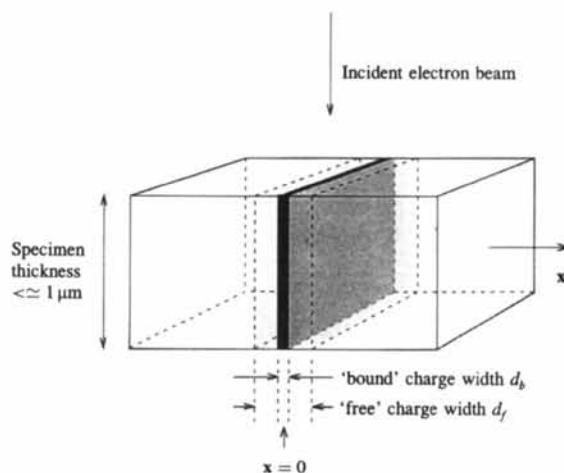


Fig. 1. Schematic diagram showing the geometry of a cross-sectional TEM specimen containing a space charge layer.

† Phase-contrast techniques are more sensitive to a local difference,  $\Delta V$ , in the mean specimen potential than to its absolute value  $V_0$ . Although  $V_0$  is affected by the presence of charged layers at specimen surfaces (O'Keeffe & Spence, 1994), it should be noted that the calculations presented here are equally applicable for determining the contribution to  $V_0$  from space charge or dipole layers on the specimen surfaces themselves.

All of the calculations of electric field, potential and force presented here are illustrated in graphical form for a hypothetical material, which has representative values for the widths and the densities of the charge distributions that are typically present at a space charge layer. In particular, the total charge number density chosen for this material corresponds to approximately 10% of one atomic layer (were it all in a single sheet) in a typical semiconductor, which is the upper limit for electrically active dopant concentrations that have been reported in delta-doped layers. The details of the other parameters chosen are given below.

For simplicity, the total charge density in the calculations is specified as a superposition of one positive and one negative charge distribution and the effect on the potential of changing the form of each charge distribution is examined. This is of particular importance because the exponential dependence that is predicted for the decrease of the defect or solute charge density with distance from an interface, originally formulated for space charge layers at free surfaces, relies on the presence of an infinite source of charged defects at the boundary (Frenkel, 1946). This condition may not always be satisfied. For example, a Gaussian distribution is more representative of both the impurity diffusion profile and the form of the ground-state free carrier wavefunction in a delta-doped semiconductor (Ploog, Hauser & Fischer, 1988) and may also be a more appropriate description for the forms of charged solute distributions at certain types of grain boundary.

In the present work, the effect of the 'fringing' fields outside a TEM foil of finite thickness is ignored. This effect has been investigated by Pozzi (1979) and Frabboni, Matteucci, Pozzi & Vanzi (1985) using Lorentz microscopy and electron holography and will be discussed in more detail in paper II of this series. It is also assumed that the electron beam does not modify the charge distribution within the specimen in any way, and for simplicity the material is treated as an isotropic continuum both electrically and mechanically

## 2. The use of a classical electrostatic potential

In high-energy electron diffraction (HEED), an incident electron is generally described using the steady-state solution of a time-independent Schrödinger equation that includes relativistic values for the mass and the wavelength of the electron but ignores the effects of spin (Fujiwara, 1962; Hirsch, Howie, Nicholson, Pashley & Whelan, 1965). Exchange-correlation forces are ignored (Saldin & Spence, 1994) and contributions from virtual inelastic scattering have been shown to be negligible (Rez, 1978). Poisson's equation is then used to relate the Hartree potential within the specimen  $V(r)$  (which is positive with maxima at the atomic positions) directly to the ground-state charge density. We assume that the above assumptions are valid for the current problem

and we also follow the approach of O'Keeffe & Spence (1994) in using classical electrostatics at distances that are of the order of interatomic spacings. Quantum-mechanical calculations of charge distributions at interlayers are then only referred to in order to determine theoretical electrostatic potentials for comparison with experimentally measured potential profiles.

It should be noted that the use of a continuum model to determine the local change in electrostatic potential and the stress at a space charge layer in a dielectric strictly requires the electric field to vary slowly over several atomic diameters. For example, both Finnis (1991) and Stoneham & Tasker (1987) have shown that a continuum approach is only valid to within about 0.25 nm of a metal/ceramic interface. The continuum model is clearly pushed to the limit of its applicability in the present work and while the results are thus unlikely to be quantitatively exact for the narrowest charge distributions they are intended to be strongly indicative of the magnitudes and the directions of the effects that are reported.

## 3. Charge, electric field, potential and force at an undepleted charged layer

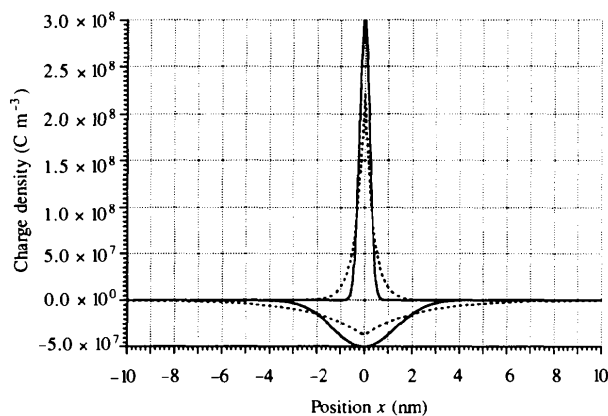
We describe a space charge layer in terms of a 'bound' charge distribution (usually consisting of solute atoms or vacancies) of density  $\rho_b(x)$  and a wider 'free' charge distribution of density  $\rho_f(x)$ , where  $\rho_b(x)$  and  $\rho_f(x)$  are each positive functions that vary only with  $x$  (the direction normal to the interface plane), are symmetrical about the centre of the layer (at  $x = 0$ ) and for which the total charge density,  $\int_{-\infty}^{+\infty} [\rho_b(x) - \rho_f(x)] dx$ , is zero as a result of overall charge neutrality. Fig. 2 shows examples of exponential and Gaussian distributions for both  $\rho_b(x)$  and  $\rho_f(x)$ , which have widths (full widths at half-maximum)  $d_b$  and  $d_f$  of 0.5 and 3.0 nm, respectively, and total projected\* charge number densities  $N_{2D}$  of  $10^{18} \text{ m}^{-2}$ . The magnitudes of these parameters correspond to representative values for space charge layers (Schubert, 1993), with the value for  $N_{2D}$  being equivalent to a charge number density of approximately 10% of one atomic layer in a semiconductor such as Si or GaAs. The charge distributions shown in Fig. 2 will be used to illustrate the effect of the form of the charge distribution on all subsequent calculations of the potential and the force at a space charge layer, and hence on the phase contrast that may be observed in the TEM. The analytical forms of all of the graphs are given in Table 1, with illustrative numerical values for some parameters in Table 2; these are intended for reference when measured potentials are related to charge distributions.

For materials that are linear isotropic dielectrics, reductions in the Coulomb force caused by the electronic

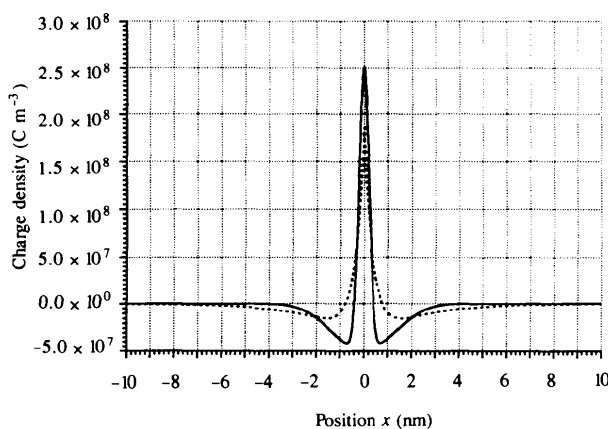
\* This is the total charge number density in the positive and negative charge distributions, were each in a single sheet.

polarization of the medium are included by the use of a single dielectric constant  $\epsilon_r$  and no further screening effects need be considered once the initial charge distributions have been specified. It should be noted that for the solution of Poisson's equation  $\nabla \cdot \mathbf{D} = \rho(\mathbf{r})$  (where the electric flux density  $\mathbf{D} = \epsilon_0 \epsilon_r \mathbf{E}$  and the electric field  $\mathbf{E} = \nabla \times \mathbf{V}$ ),  $\mathbf{D}$  does not in general depend merely on  $\rho(\mathbf{r})$  but also on the boundary conditions. In the absence of externally applied fields, and for a total charge of zero and a symmetrical charge distribution, the electric field associated with a layer of charge density  $\rho(x) = \rho_b(x) - \rho_f(x)$  must tend to zero both at large distances from the interlayer and at its centre. Therefore,

$$\begin{aligned} E(x) &= (-1/\epsilon_0 \epsilon_r) \int_x^\infty \rho(u) du \\ &\equiv (1/\epsilon_0 \epsilon_r) \int_0^x \rho(u) du \end{aligned}$$



(a)



(b)

Fig. 2. Examples of (a) individual and (b) total charge distributions at a space charge layer. The 'bound' and 'free' charge distributions shown have full widths at half-maximum  $d_b$  and  $d_f$  of 0.5 and 3.0 nm, respectively. Gaussian and exponential charge distributions are shown using solid and broken lines, respectively.

and

$$V(x) = \int_x^\infty E(v) dv = (1/\epsilon_0 \epsilon_r) \int_{v=x}^\infty dv \int_{u=0}^v \rho(u) du,$$

where  $V(\pm\infty) = 0$  and  $V(0)$  can also be written in the form of a dipole moment per unit area as

$$V(0) = (-1/\epsilon_0 \epsilon_r) \int_0^\infty u \rho(u) du$$

(Landau & Lifshitz, 1960). Expressions for the field and potential obtained in this way are given in Table 2 for both exponential and Gaussian charge-density distributions. The qualitative interpretation of the sense (the sign) of a TEM-measured potential is important and can be understood as follows. For an isolated atom, which corresponds to a localized region of positive charge and a wider distribution of negative charge, the spatially averaged potential is positive. Correspondingly, a space charge layer consisting of positive ions surrounded by negative free carriers will raise the value of  $V_0$  and *vice versa*. Fig. 3 shows the calculated electric field and potential corresponding to the charge distributions shown in Fig. 2 for a material with a dielectric constant  $\epsilon_r$  of 10. This value for the dielectric constant is again typical for a semiconductor such as Si or GaAs. Several important points are apparent from Fig. 3(b):

(i) The magnitude of the change in potential is much greater than the detection limit of approximately 0.05 V for the measurement of potential variations that have widths of a few nm or less using Fresnel contrast analysis (Ross & Stobbs, 1991). According to the relations given in Table 2, this detection limit would suggest that a space charge layer can be detected using Fresnel contrast analysis if the parameter

$$[N_{2D}(d_f - d_b)]/\epsilon_r$$

is greater than  $1.6 \times 10^7$  and  $7.7 \times 10^6 \text{ m}^{-1}$  for Gaussian and exponential charge distributions, respectively. For Si ( $\epsilon_r = 11.9$ ) with  $d_f - d_b$  taking a value of 3 nm, the detection limits would correspond to total projected charge number densities of 0.9 and 0.4% of one atomic layer for space charge layers having Gaussian and exponential charge distributions, respectively.

(ii) There is clearly a dramatic difference in both the magnitude  $V(0)$  and the width  $w_0$  of the electrostatic potential at a space charge layer when the shapes of the original charge distributions are changed while the values of  $d_b$ ,  $d_f$  and  $N_{2D}$  are held constant. The larger potential is associated with a charge distribution that has a longer tail and this illustrates the extreme care that is necessary when relating a measured potential to an assumed form for the charge distributions. The same effect has been discussed by O'Keeffe & Spence (1994) and Davis *et al.* (1995) in the different context of relating the absolute magnitudes of mean forward-

Table 1. Summary of expressions (analytical where available, otherwise in their simplest form) for an isotropic material, for both Gaussian and exponential charge distributions

	Gaussian	Exponential
Charge densities		
Total charge density	$\rho_G(x) = A \exp(-\alpha x^2) - B \exp(-\beta x^2)$	$\rho_E(\mathbf{x}) = C \exp(-\gamma \mathbf{x} ) - D \exp(-\delta \mathbf{x} )$
Definitions of constants (all positive)	$\alpha = \frac{4 \ln 2}{d_b^2} \quad \beta = \frac{4 \ln 2}{d_f^2} \quad A = \frac{2eN_{2D}}{d_b} \left( \frac{\ln 2}{\pi} \right)^{1/2} \quad B = \frac{2eN_{2D}}{d_f} \left( \frac{\ln 2}{\pi} \right)^{1/2}$	$\gamma = \frac{2 \ln 2}{d_b} \quad \delta = \frac{2 \ln 2}{d_f} \quad C = \frac{\ln 2eN_{2D}}{d_b} \quad D = \frac{\ln 2eN_{2D}}{d_f}$
Electrostatic potential	$V(x) = \left( \frac{1}{\epsilon_0 \epsilon_r} \right) \left( \frac{\pi \right)^{1/2} \int_0^x \left\{ \frac{A}{(\alpha)^{1/2}} \operatorname{erf}[u(\alpha)^{1/2}] - \frac{B}{(\beta)^{1/2}} \operatorname{erf}(u\beta) \right\} du$ $\equiv 9.0476 \times 10^{-9} \left( \frac{N_{2D}}{\epsilon_r} \right) \int_0^x \left\{ \operatorname{erf} \left[ 2(\ln 2)^{1/2} \frac{ u }{d_b} \right] - \operatorname{erf} \left[ 2(\ln 2)^{1/2} \frac{ u }{d_f} \right] \right\} du$	$V(\mathbf{x}) = \left( \frac{1}{\epsilon_0 \epsilon_r} \right) \left[ \frac{D}{\delta^2} \exp(-\delta \mathbf{x} ) - \frac{C}{\gamma^2} \exp(-\gamma \mathbf{x} ) \right]$ $\equiv 6.5264 \times 10^{-9} \left( \frac{N_{2D}}{\epsilon_r} \right) \left[ d_f \exp \left( \frac{-2 \ln 2 \mathbf{x} }{d_f} \right) - d_b \exp \left( \frac{-2 \ln 2 \mathbf{x} }{d_b} \right) \right]$
Potential at centre of layer	$V(0) = \left( \frac{1}{\epsilon_0 \epsilon_r} \right) \left( \frac{B}{2\beta} - \frac{A}{2\alpha} \right) \equiv 3.0656 \times 10^{-9} \left( \frac{N_{2D}}{\epsilon_r} \right) (d_f - d_b)$	$V(0) = \left( \frac{1}{\epsilon_0 \epsilon_r} \right) \left( \frac{D}{\delta^2} - \frac{C}{\gamma^2} \right) \equiv 6.5264 \times 10^{-9} \left( \frac{N_{2D}}{\epsilon_r} \right) (d_f - d_b)$
Width of potential (FWHM)*	No analytical solution. The least-squares biquadratic fit to the true values (accurate to better than 2.4% for $0 \leq d_b < d_f \leq 10^{-8}$ m) is $w_0 = 1.06 \times 10^{-12} + 0.592d_b + 0.424d_f + 9.56 \times 10^6 d_b d_f - 9.64 \times 10^6 d_b^2 - 1.56 \times 10^6 d_f^2$	No analytical solution. The least-squares biquadratic fit to the true values (accurate to better than 2.0% for $0 \leq d_b < d_f \leq 10^{-8}$ m) is $w_0 = 3.92 \times 10^{-12} + 1.43d_b + 1.03d_f + 3.18 \times 10^7 d_b d_f - 3.19 \times 10^7 d_b^2 - 5.28 \times 10^6 d_f^2$
Electric field	$E(x) = \left( \frac{1}{\epsilon_0 \epsilon_r} \right) \left( \frac{\pi \right)^{1/2} \left\{ \frac{A}{(\alpha)^{1/2}} \operatorname{erf}[x(\alpha)^{1/2}] - \frac{B}{(\beta)^{1/2}} \operatorname{erf}[x(\beta)^{1/2}] \right\}$ $\equiv 9.0476 \times 10^{-9} \left( \frac{N_{2D}}{\epsilon_r} \right) \left\{ \operatorname{erf} \left[ 2(\ln 2)^{1/2} \frac{ x }{d_b} \right] - \operatorname{erf} \left[ 2(\ln 2)^{1/2} \frac{ x }{d_f} \right] \right\}$	$E(\mathbf{x})_{x \geq 0} = \left( \frac{\pm 1}{\epsilon_0 \epsilon_r} \right) \left[ \frac{D}{\delta} \exp(-\delta \mathbf{x} ) - \frac{C}{\gamma} \exp(-\gamma \mathbf{x} ) \right]$ $\equiv \pm 9.0476 \times 10^{-9} \left( \frac{N_{2D}}{\epsilon_r} \right) \left[ \exp \left( \frac{-2 \ln 2 \mathbf{x} }{d_f} \right) - \exp \left( \frac{-2 \ln 2 \mathbf{x} }{d_b} \right) \right]$
Maximum stress within crystal	$\sigma_b = \left[ \frac{(\pi)^{1/2}}{2\epsilon_0 \epsilon_r} \right] \int_0^\infty \left\{ \frac{A}{(\alpha)^{1/2}} \operatorname{erf}[x(\alpha)^{1/2}] - \frac{B}{(\beta)^{1/2}} \operatorname{erf}[x(\beta)^{1/2}] \right\} [A \exp(-\alpha x^2)] dx$ $\equiv 1.3618 \times 10^{-27} \left[ \frac{(N_{2D})^2}{\epsilon_r} \right] \int_0^\infty \left\{ \operatorname{erf} \left[ 2(\ln 2)^{1/2} \frac{ x }{d_b} \right] - \operatorname{erf} \left[ 2(\ln 2)^{1/2} \frac{ x }{d_f} \right] \right\}$ $\times \left\{ \frac{1}{d_b} \exp \left[ -\ln 2 \left( \frac{2x}{d_b} \right)^2 \right] \right\} dx$	$\sigma_b = \left( \frac{1}{\epsilon_0 \epsilon_r} \right) \left( \frac{C^2}{2\gamma^2} - \frac{CD}{\delta(\gamma + \delta)} \right) \equiv 3.6240 \times 10^{-28} \left[ \frac{(N_{2D})^2}{\epsilon_r} \right] \left( \frac{d_f - d_b}{d_f + d_b} \right)$

Table 1 (cont.)

Strain	$\begin{aligned} \epsilon(x) &= \left( \frac{1}{Y\epsilon_0\epsilon_r} \right) \left( \frac{\pi^{1/2}}{2} \right) \int_{ x }^{\infty} \left\{ \frac{A}{(\alpha)^{1/2}} \operatorname{erf}[u(\alpha)^{1/2}] - \frac{B}{(\beta)^{1/2}} \operatorname{erf}[u(\beta)^{1/2}] \right\} \\ &\quad \times [A \exp(-\alpha u^2)] du \\ &\equiv 1.6357 \times 10^{-27} \left[ \frac{(N_{2D})^2}{Y\epsilon_r} \right] \int_{ x }^{\infty} \left\{ \operatorname{erf} \left[ 2(\ln 2)^{1/2} \frac{ u }{d_b} \right] - \operatorname{erf} \left[ 2(\ln 2)^{1/2} \frac{ u }{d_f} \right] \right\} \\ &\quad \times \left\{ \frac{1}{d_b} \exp \left[ -\ln 2 \left( \frac{2u}{d_b} \right)^2 \right] \right\} du \end{aligned}$	$\begin{aligned} \epsilon(x) &= \left( \frac{1}{Y\epsilon_0\epsilon_r} \right) \int_{ x }^{\infty} \left[ \frac{D}{\delta} \exp(-\delta u ) - \frac{C}{\gamma} \exp(-\gamma u ) \right] [C \exp(-\gamma u )] du \\ &\equiv 1.0048 \times 10^{-27} \left[ \frac{(N_{2D})^2}{\epsilon_r} \right] \int_{ x }^{\infty} \left[ \exp \left( \frac{-2 \ln 2  x }{d_b} \right) - \exp \left( \frac{-2 \ln 2  u }{d_f} \right) \right] \\ &\quad \times \left[ \frac{1}{d_b} \exp \left( \frac{-2 \ln 2  u }{d_b} \right) \right] du \end{aligned}$
Lattice expansion across layer	$\begin{aligned} \Delta l &= \left( \frac{\pi}{Y\epsilon_0\epsilon_r} \right)^{1/2} \int_{x=0}^{\infty} \int_{u=0}^{\infty} \left\{ \frac{A}{(\alpha)^{1/2}} \operatorname{erf}[u(\alpha)^{1/2}] - \frac{B}{(\beta)^{1/2}} \operatorname{erf}[u(\beta)^{1/2}] \right\} \\ &\quad \times [A \exp(-\alpha u^2)] du dx \end{aligned}$	$\begin{aligned} \Delta l &= \left( \frac{1}{\epsilon_0\epsilon_r} \right) \left( \frac{1}{Y} \right) \left[ \frac{2CD}{\delta(\gamma + \delta)^2} - \frac{C^2}{2\gamma^2} \right] \\ &\equiv 2.6141 \times 10^{-28} \left[ \frac{(N_{2D})^2}{\epsilon_r Y} \right] \left[ \frac{d_b(3d_f + d_b)(d_f - d_b)}{(d_f + d_b)^2} \right] \end{aligned}$

\* Full width at half-maximum.

Table 2. Numerical solutions for an isotropic material with parameters  $N_{2D} = 10^{18} \text{ m}^{-2}$ ,  $d_b = 0.5$ ,  $d_f = 3.0 \text{ nm}$ ,  $\epsilon_r = 10$  and  $Y = 10^{11} \text{ N m}^{-2}$ , for both Gaussian and exponential charge distributions

$d_b$  and  $d_f$  are the full widths at half-maximum of the bound and free charge distributions, respectively,  $N_{2D}$  is the total projected positive or negative charge number density,  $\epsilon_r$  is the dielectric constant and  $Y$  is Young's modulus. SI units have been used throughout.

Forms of individual charge distributions	Gaussian	Exponential
Potential at centre of layer (V)	0.77	1.6
Width of potential (m)	$1.6 \times 10^{-9}$	$3.8 \times 10^{-9}$
Maximum stress within crystal ( $\text{N m}^{-2}$ )	$2.9 \times 10^7$	$2.6 \times 10^7$
Rigid lattice expansion (m)	$1.3 \times 10^{-13}$	$2.5 \times 10^{-13}$

scattering potentials to the extents of electron-density distributions around individual atoms.

(iii) The relations in Table 2 also indicate that for a given form of the charge distributions the magnitude of the potential  $V(0)$  is directly proportional to  $N_{2D}(d_f - d_b)$  and its width  $w_0$  is a function of  $d_f$  and  $d_b$  only. The parameters  $d_f$  and  $N_{2D}$  can thus be determined if a value for  $d_b$  is either assumed or measured independently. In addition, for a delta-doped layer in a semiconductor that has a bound charge distribution of width less than approximately 2 nm, a self-consistent solution of the Schrödinger and Poisson equations indicates that the spatial extent of the ground-state free-carrier wavefunction is

$$z_0 = 2(7/5)^{1/2} \left( \frac{\hbar^2 \epsilon_0 \epsilon_r}{9\pi^2 e^2 m^* N_{2D}} \right)^{1/3},$$

where  $m^*$  is the free carrier effective mass (Schubert, 1993). If this expression for  $z_0$  (which may also be valid for certain grain boundaries) can be related to  $d_f$  then  $N_{2D}$ ,  $d_f$  and  $d_b$  can all be determined from experimental measurements of  $V_0$  and  $w_0$ .

The strain within a material is also an important parameter for the interpretation of TEM contrast. The electrostatic contribution to the strain at a space charge layer results from electrostatic attraction of the 'bound' charge (the narrower charge distribution) to the 'free' charge (the wider charge distribution). A region of 'bound' charge of width  $dx$  at position  $x$ , containing net charge per unit area  $\rho_b(x) dx$ , experiences an electrostatic force per unit area of magnitude

$$d\sigma_b(x) = \rho_b(x)E(x) dx = [\rho_b(x)dx/\epsilon_0\epsilon_r] \int_0^x \rho(u) du$$

[ $E(x)$  in this expression is associated with charges external to the layer being considered]. This contribution to the force is directed away from the centre of the layer, is zero at its centre and always results in an expansion

of the lattice (so long as  $d_f > d_b$ ). The bound charge is thus drawn out and the free charge in, since equalizing the two distributions would cancel the charge completely and so minimize the electrostatic energy per unit area,

$$\frac{1}{2} \epsilon_0 \epsilon_r \int_{-\infty}^{\infty} [E(x)]^2 dx,$$

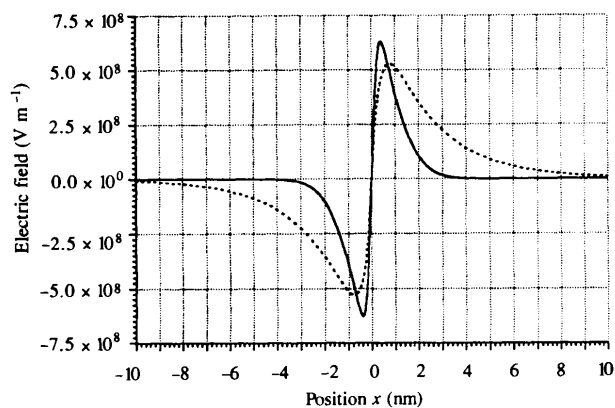
at a value of zero. The force per unit volume (*i.e.* the gradient of the force per unit area)  $d\sigma_b/dx$  is plotted in Fig. 4(a) for the charge distributions in Fig. 2 and again for a material that has a dielectric constant  $\epsilon_r$  of 10. As long as the material is free to relax parallel to the interface, the contribution to the strain at each such position is thus

$$\epsilon(x) = \sigma(x)/Y = (1/Y) \int_x^{\infty} \rho_b(u) E(u) du,$$

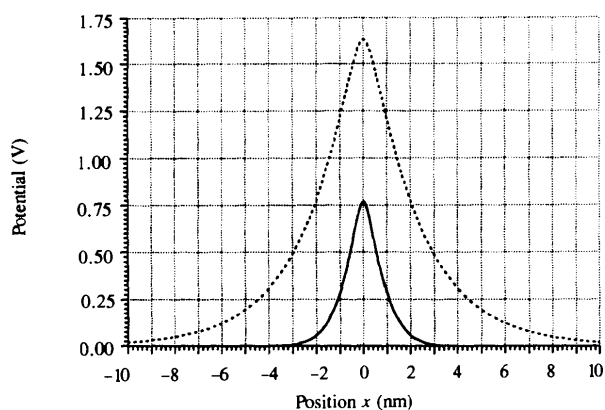
where the maximum value of the stress  $\sigma(x)$  is  $\sigma_b$  at  $x = 0$ ,  $Y$  is Young's modulus and the material is assumed

to be isotropic. The electrostatic contribution to the strain for the charge distribution shown in Fig. 2, for a material with representative values  $\epsilon_r$  of 10 and  $Y$  of  $10^{11} \text{ N m}^{-2}$ , is shown in Fig. 4(b) and is much more localized than the extent of the electrostatic potential in Fig. 3. It is clear from Fig. 4(b) that the magnitude of the strain is negligible when compared with the typical magnitudes of strains that are associated with compositional fluctuations (*i.e.* changes in ionic radii) at a boundary and is too small to affect  $V_0$  appreciably. However, the total rigid lattice shift,  $\Delta l_{\text{tot}}$ , of the crystal lattice across such a space charge layer is a parameter that can be measured accurately using the technique of regression analysis (Stobbs, Wood & Smith, 1984). The magnitude of the electrostatic contribution to  $\Delta l_{\text{tot}}$  is

$$\Delta l = 2 \int_0^{\infty} \epsilon(x) dx = (2/Y) \int_{x=0}^{\infty} dx \int_{u=x}^{\infty} \rho_b(u) E(u) du.$$

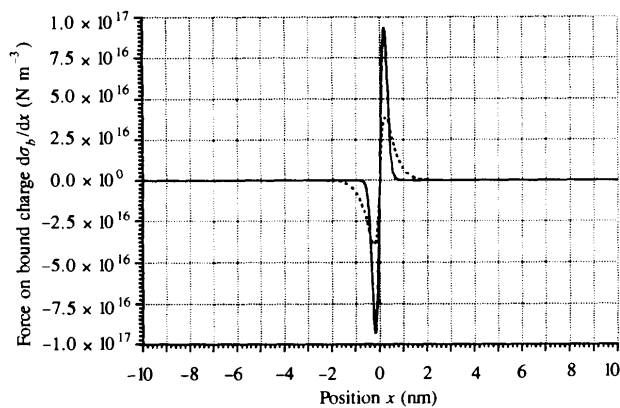


(a)

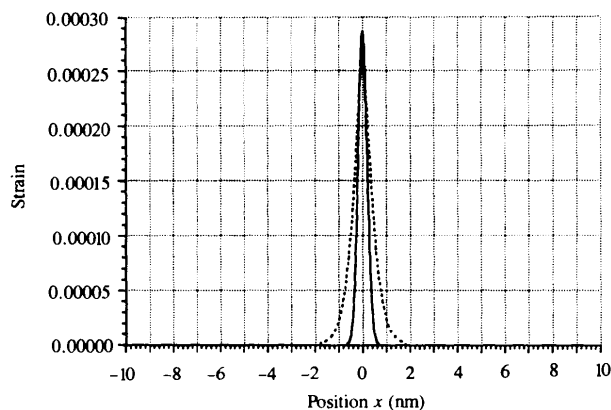


(b)

Fig. 3. (a) Electric field and (b) electrostatic potential for the charge distributions depicted in Fig. 2 for an isotropic material with a dielectric constant  $\epsilon_r$  of 10. A change in the direction of the electric field is shown using a change of sign. Gaussian and exponential charge distributions are shown using solid and broken lines, respectively.



(a)



(b)

Fig. 4. Electrostatic contributions to (a) the force acting on the bound charge and (b) the strain within the material at a space charge layer for the charge distributions depicted in Fig. 2 and for an isotropic material with a dielectric constant  $\epsilon_r$  of 10 and a Young's modulus  $Y$  of  $10^{11} \text{ N m}^{-2}$ . A change in the direction of the force is shown using a change of sign. Gaussian and exponential charge distributions are shown using solid and broken lines, respectively.

Values are given in Table 1 for the Gaussian and exponential charge distributions and the representative values of  $d_b$ ,  $d_f$ ,  $N_{2D}$ ,  $Y$  and  $\epsilon_r$  chosen for the previous calculations. The magnitude of this contribution to the rigid lattice shift, at approximately  $10^{-13}$  m for the parameters chosen, is also too small to be measured using regression analysis, which has a detection limit of approximately  $10^{-12}$  m.

#### 4. Conclusions

The electrostatic potential and strain at a space charge layer in an isotropic material have been determined using classical electrostatics. This will allow the magnitude and the width of a TEM-measured electrostatic potential to be related directly to the widths and the concentrations of the charge distributions within a material. The form of the charge distribution has been shown to affect the potential distribution strongly. Both the rigid lattice expansion and the strain associated with the presence of the charge distribution have been shown to be small. The relations presented here may also prove useful for explaining results obtained for charged layers using techniques such as scanning electron microscopy (Perovic *et al.*, 1995), scanning tunnelling microscopy (Bonnell & Solomon, 1992) and X-ray diffraction (Fewster, 1993).

We are grateful to Dr D. D. Perovic and Dr C. B. Boothroyd for discussions, and the EPSRC (RED) and the Isaac Newton Trust and Synoptics Ltd (WOS) for financial support.

#### References

- Bonnell, D. A. & Solomon, I. (1992). *Ultramicroscopy*, **42**, 788–792.
- Davis, C. A., Silva, S. R. P., Dunin-Borkowski, R. E., Amaratunga, G. A. J., Knowles, K. M. & Stobbs, W. M. (1995). *Phys. Rev. Lett.* **75**, 4258–4261.
- Dunin-Borkowski, R. E., Stobbs, W. M., Perovic, D. D. & Wasilewski, Z. R. (1994). *Proceedings of ICEM13*, edited by B. Jouffrey & C. Colliex, Vol. 1, pp. 411–412. Paris: Les Editions de Physique.
- Fewster, P. F. (1993). *Semicond. Sci. Technol.* **8**, 1915–1934.
- Finnis, M. W. (1991). *Surf. Sci.* **241**, 61–72.
- Frabboni, S., Matteucci, G., Pozzi, G. & Vanzi, M. (1985). *Phys. Rev. Lett.* **55**, 2196–2199.
- Frenkel, J. (1946). *Kinetic Theory of Liquids*, pp. 36–40. New York: Dover.
- Fujiwara, K. (1962). *J. Phys. Soc. Jpn*, **17** (Suppl. BII), 118.
- Hirsch, P. B., Howie, A., Nicholson, R. B., Pashley, D. W. & Whelan, M. J. (1965). *Electron Microscopy of Thin Crystals*. London: Butterworths.
- Ikeda, J. A. S. & Chiang, Y.-M. (1993). *J. Am. Ceram. Soc.* **76**, 2437–2446.
- Ikeda, J. A. S., Chiang, Y.-M., Garratt-Reed, A. J. & Vander Sande, J. B. (1993). *J. Am. Ceram. Soc.* **76**, 2447–2459.
- Landau, L. D. & Lifshitz, E. M. (1960). *Electrodynamics of Continuous Media*, p. 99. Oxford: Pergamon Press.
- Lin, X., Ravikumar, V., Rodrigues, R. P., Wilcox, N. & David, V. P. (1995). In *Electron Holography*. Elsevier Science, Delta Series. Amsterdam: Elsevier.
- O’Keeffe, M. & Spence, J. C. H. (1994). *Acta Cryst.* **A50**, 33–45.
- Perovic, D. D., Castell, M. R., Howie, A., Lavoie, C., Tiedje, T. & Cole, J. S. W. (1995). *Ultramicroscopy*, **58**, 104–113.
- Ploog, K., Hauser, M. & Fischer, A. (1988). *Appl. Phys.* **A45**, 233–244.
- Pozzi, G. (1979). *Optik (Stuttgart)*, **53**, 381–394.
- Rez, P. (1978). *Acta Cryst.* **A34**, 48–51.
- Ross, F. M. & Stobbs, W. M. (1991). *Philos. Mag.* **A63**, 1–36, 37–70.
- Saldin, D. K. & Spence, J. C. H. (1994). *Ultramicroscopy*, **55**, 397–406.
- Schubert, E. F. (1993). *Doping in III–V Semiconductors*, pp. 433–481. Cambridge University Press.
- Stobbs, W. M., Wood, G. J. & Smith, D. J. (1984). *Ultramicroscopy*, **14**, 145–154.
- Stoneham, A. M. & Tasker, P. W. (1987). *Philos. Mag.* **B55**, 237–252.
- Tonomura, A. (1992). *Adv. Phys.* **41**, 59–103.
- Yan, M. F., Cannon, R. M. & Bowen, H. K. (1983). *J. Appl. Phys.* **54**, 764–778.